EUROPEAN FUSION DEVELOPMENT AGREEMENT

EFDA–JET–PR(01)123

M.F.F. Nave et al

Control of Impurity Accumulation in JET Radiative Mantle Discharges

Control of Impurity Accumulation in JET Radiative Mantle Discharges

M.F.F.Nave[1], J.Rapp[2], T.Bolzonella[3], R.Dux[4], M.J.Mantsinen[7], R.Budny[9], P.Dumortier[8], M. von Hellermann[10], S Jachmich[2], H.R. Koslowski[2], G. Maddison[5], A.Messiaen[8], P.Monier-Garbet[6], J.Ongena[8], M.E.Puiatti[3], J.Strachan[9], G.Telesca[8], B.Unterberg[2], M.Valisa[3], and contributors to the EFDA-JET workprogramme*

[1]Associação EURATOM/IST, Centro de Fusão Nuclear, 1049-001 Lisbon, Portugal
[2]Association EURATOM-FZ-Juelich, Institut fuer Plasmaphysik, TEC, 52425 Juelich, Germany
[3]Consorzio RFX - Associazione Euratom-Enea sulla Fusione, Corso Stati Uniti 4, I-35127 Padova, Italy
[4]Max-Planck-Institut für Plasmaphysik, IPP-EURATOM Assoziation, Boltzmann-Str.2, D-85748 Garching
[5]Euratom/UKAEA Fusion Association, Culham Science Centre, Abingdon, OX14 3DB, UK
[6]Association EURATOM/CEA CEA Cadarache, DRFC, Bâtiment 513, 13108 Saint-Paul-Lez-Durance, France
[7]Helsinki University of Technology, Association Euratom-Tekes, P.O.Box 2200, FIN-02015 HUT, Finland
[8]LPP-ERM/KMS, Association Euratom-Belgian State, Brussels, Belgium
[9]PPPL, Princeton University, N.J., USA
[10]FOM, Rijnhuizen, NL
**see appendix of the paper by J. Pamela "Overview of recent JET results", Proc. IAEA conference on Fusion Energy, Sorrento, 2000*

ABSTRACT

Impurity injection in the JET ELMy H-mode regime has produced high confinement, quasi-steady state plasmas with densities close to the Greenwald density. However, at large Ar densities, a sudden loss of confinement is observed. A possible correlation between loss of confinement and the observed MHD phenomena both in the core and the edge of the plasma was considered. The degradation in confinement coincides with impurity profile peaking following the disappearance of sawtooth activity. Experiments were designed to understand the role of sawtooth crashes in re-distributing impurities. ICRF heating was used to maintain sawtooth activity and resulted in quasi-steady state, high performance plasmas with high Ar densities. At $H_{97}*f_{GWD}$~0.8 and high Ar injection rates, quasi-steady states which previously only lasted <1 τ_E, were now maintained for the duration of the heating (Δt~9τ_E). We conclude that sawtooth activity plays an important role in preventing impurity accumulation.

I . INTRODUCTION

Injection of high-Z impurities to create a cool radiative mantle around the plasma has been a successful technique used in the TEXTOR [1-3] and DIII-D [4] tokamaks to improve the level of confinement in high-density regimes. Experiments performed at JET [5-7] and JT60 [8] in recent years tested this technique in large machines. JET radiative mantle experiments in the ELMy H-mode regime, produced high confinement quasi-steady state plasmas with high confinement (H_{97}~1) and densities close to the Greenwald density ($n/n_{GWD}\geq 0.85$) [6] as required for the future operation of ITER [9]. JET radiative mantle experiments have been mainly performed in divertor plasmas, following two main lines of thought: a) L-mode plasmas, heated by Neutral Beam Injection (NBI) before the plasma current is fully penetrated [10], similar to DIII-D experiments [4]; b) ELMy-H mode plasmas, heated by NBI during the current flat top [6]. This paper describes the work done to understand the loss of confinement and the measures taken to improve stationarity of ELMy H-mode discharges with high radiation fractions ($\gamma=P_{rad}/P_{tot}>0.7$) from Argon (Ar) injection. We consider discharges obtained in the septum configuration [11], i.e. discharges with the X-point embedded in the dome of the JET MKIIGB divertor [12]. The septum radiative mantle experiments of JET share many characteristics with the limiter Radiative Improved (RI) modes of TEXTOR [1]. As in TEXTOR, JET experiments show that higher densities can be achieved in discharges with increased radiation level, when compared with discharges without impurity injection [6]. However, unlike TEXTOR where 30% confinement improvements were observed, moderate impurity injection levels at JET ($\phi_{Ar}<4x10^{21}$el/s) maintained H_{97}~1 but at higher densities. With larger impurity injection rates confinement is reduced. One TEXTOR RI-mode characteristic was a peaked plasma current distribution compared to the unseeded case, and a low central q-factor (q(0) could be as small as 0.6) [13]. When impurity puffing ended, q(0) increased and after a transient improvement, confinement decreased. Both JET and TEXTOR experiments indicated that control of the central current density and core MHD stability may maintain the good confinement phase. Central MHD

activity in TEXTOR RI-modes [13] and JET radiative mantle ELMy H-modes [14] are similar. This paper shows that by controlling q(0) and core MHD activity, the good confinement phase of JET radiative mantle discharges was prolonged. One difference between TEXTOR and JET experiments was the edge conditions. TEXTOR confinement improvement arises from the plasma core, while JET radiative mantle experiments combine good core confinement with edge H-mode confinement. Therefore, edge stability and ELM behaviour were important in JET plasmas and contribute to maintain good confinement.Section II, below, describes observations in the septum discharges with high impurity densities. The correlation between confinement loss and MHD phenomena are described for the core in section III and the edge of the plasma in section IV. The degradation correlated with two main phenomena: a) Ar accumulation in the plasma core and, b) disappearance of sawtooth activity. Experiments designed to understand the role of sawtooth crashes in re-distributing impurities are reported in section V. Control of sawteeth activity with ion-cyclotron radio frequency heating (ICRH) resulted in quasi-steady state, high performance. Further benefits of increasing heating in the plasma core are discussed in section VI.

II. CONFINEMENT LOSS AT HIGH IMPURITY INJECTION

In the septum configuration, the highest performance plasmas ($H_{97}*f_{GWD} \geq 0.8$) were obtained with 12 MW NBI heating, with two gas injection phases: an initial phase of continuous D_2 and Ar fuelling, followed by the "after-puff" phase when both gases' injection rates were reduced. In the after-puff phase, confinement improved for 1-2 s, then either saturated or declined. In discharges with low or moderate Ar seeding, a quasi-steady state regime remained through to the end of the applied heating [6]. However, at higher Ar injection rates ($\phi_{Ar} \geq 4x10^{21}$ el/s), the high confinement phase was transient (fig.1).

In the puff phase (fig.1), high deuterium fuelling was used to increase the density, while the radiation level was also increased by Ar injection. At this high level of fuelling, the energy confinement time decreased (fig. 1). In the after-puff phase the D_2 puff is reduced or stopped, while Ar injection continued at lower level. Confinement increased to its previous H-mode level. Several MHD changes occurred in the after-puff phase. On the core, sawtooth amplitude decreased, as normally observed at high core density. The sawtooth crashes stop (1.3 s in fig.1.). The central temperature signal and the magnetic pick-up coil signal, where the spikes corresponding to sawtooth pre-cursors are observed, were indicators of sawtooth MHD activity. Edge stability has also changed. The type III ELM regime observed during the puff phase changed to type I ELMs. In the after-puff phase, energy confinement degradation coincided with Ar accumulation in the plasma core (1.5 sec in fig.1). Further energy confinement loss occurred due to core radiative collapse (2.3 sec in fig.1, discussed later in section VI).

The phenomenology just described was similar at lower impurity injection. Impurity density peaking and sawtooth suppression were observed (see section III). However with lower central impurity concentrations, the confinement degradation was not observed. Energy confinement is however limited,

saturating at a level generally below that observed in reference discharges without Ar [6].

The impurity accumulation correlated in time with both the sawtooth suppression and the ELM changes (fig. 1). Thus the central impurity peaking might be correlated with either / or both the change in central or edge MHD activity. Analysis of impurity densities from many discharges indicated that impurity peaking occurred independently from ELM repetition frequency (see section IV), while a correlation was found between impurity peaking and sawtooth suppression (section III).

The temporal evolution of the central Ar density was derived from bolometry measurements for 50 discharges. The bolometer signals in the upper half of the poloidal cross section were Abel inverted with the assumption of a poloidally symmetric radiation distribution. The core Ar was assumed to be in coronal equilibrium. Thus the Ar concentration on axis was using the cooling rates, L_u, from Post [15], where n_e is the electron density and T_e the electron temperature.

$$C_{Ar} = \frac{P_{rad}(0)}{n_e(0)^2 L_u(T_e(0))}$$

For a smaller number of discharges, with low to moderated Ar levels, impurity density profiles were obtained from analysis of Soft-X Ray (SXR) emission profiles, as explained in the next section.

III. IMPURITY PEAKING AND SAWTOOTH OBSERVATIONS

The sawtooth period and amplitude observed in the radiative mantle discharges followed the empirical relations obtained for non-seeded JET H-modes with NBI heating, described in [16]. The scaling of sawtooth properties with plasma parameters has been obtained at JET by a regression analysis from over 300 discharges indicating that the sawtooth period was proportional to: $T_e^{1.7}\, n_e^{0.23}$, while the amplitude was proportional to: $n_e^{-0.53} q_{95}^{-0.98} p_p^{0.23} \delta^{0.23}\, (\kappa\text{-}1)^{-1.8}$ (where p_p is the pressure profile peaking factor, n_e and T_e are the central electron density and temperature). Thus the reduction in sawtooth amplitude observed in the after-puff phase is typical of discharges with a high core density. Slow impurity accumulation in the plasma core was observed when sawtooth crashes have reduced amplitude. In discharges with a high Ar input, as in figure 1, a sudden increase in central impurity concentration followed the disappearance of sawtooth activity. The time of sudden impurity accumulation (t_{imp} in fig. 1) equaled the time of the last sawtooth crash within $\pm$ 0.3 sec with a range of 10 sec (fig. 2). In most cases this increase in C_{Ar} was observed in the after-puff phase, however in a few cases, both sawtooth suppression and impurity accumulation were observed in the puffing phase.

Central radiation increase and impurity accumulation were not seen in discharges where central MHD modes, sawteeth and/or continuous (m=1,n=1) modes, were observed up to the end of the after-puff phase. With P_{NBI}=12 MW, central n=1 modes remaining to the end of the heating phase were seen in unseeded discharges and occasionally in seeded discharges with a low Ar injection rate. Two discharges with low Ar injection rate (ϕ_{Ar} ~1x10^{21} el/s) that showed different sawtooth behavior are compared in figure 3. With the sawteeth activity maintained (fig.3 top), no central radiation peaking is observed. In fig.3 (bottom), sawteeth were suppressed at t~2s whilst a continuous central (m=1, n=1) lasted until t~3.5 s. The central radiation started to increase at the disappearance

of the sawtooth. The radiation profile became more peaked once the central n=1 mode disappeared. The observation that sawtooth-free periods coincide with core impurity accumulation was similar to observations from ASDEX [17], ASDEX-Upgrade [18-19] and TEXTOR [20]. In ASDEX-Upgrade the absence of sawtooth and fishbone' relaxations correlated with an increase in central SXR emission and indicated an impurity density increase. Those experiments suggested that sawteeth and other central MHD modes contributed to impurity profile control. SXR analysis of JET radiative mantle discharges, reported here, lead to similar conclusions.

Typically, q(0)~0.9 in the puff phase (EFIT code equilibrium reconstruction [21]). Once the gas rate was decreased, q(0) increased and sawtooth suppression occurred when q(0) rose above unity (figure 1). The q(0) rose due to an increase in edge pedestal temperature in the after puff phase. The resistivity at the plasma edge decreased and the plasma current was re-distributed, leading to an increased edge plasma current density and consequently to a reduced central plasma current density. By contrast, the current density profile became very peaked during the TEXTOR RI-Mode high confinement phase [13], due to the radiating belt with an L-Mode edge. However, also at TEXTOR when the impurity seeding was stopped, q(0) was in some cases observed to rise above unity [13]. At JET the magnetic equilibrium reconstruction as well as MHD mode analysis [14] indicated that the central q-profile was nearly flat and close to unity near the time of sawtooth suppression. After sawtooth suppression, equilibrium reconstruction with polarimetric measurements indicated reversed shear q-profiles (fig. 4). The central q(0) evolution after q>1 , not observed in non-seeded discharges, was plausibly a result of impurity accumulation. When the central q profile was flat and close to unity, the (m=1, n=1) precursor mode associated with sawteeth was a continuous mode (fig. 3, top). The core MHD modes observed are similar to those reported from TEXTOR [13] when q(0) was close to unity. Reversed shear, associated with impurity accumulation, was also seen in TEXTOR [13, 20] in accumulation studies of high-Z impurities in radiation-cooled discharges. At JET, if the central q was non-monotonic and above unity, (m=4, n=3) and (m=3, n=2) modes may become unstable. The (m=3, n=2) modes limited core density [14].

On axis ICRH (Figures 5 and 6) altered the q(0) evolution so that the sawtooth instability was maintained throughout the heating phase in discharges with moderate to high impurity injection (section V). The increased sawtooth period due to ICRH fast particle effects, allowed us to study the effect of sawtooth crashes on the evolution of the Ar profiles, obtained from SXR analysis, in a discharge where the sawtooth repetition frequency was quite low. The sawtooth crash redistributed impurities (fig.5). In the fuelling phase (–1 to 0 sec in fig.5) the central impurity density increased at each sawtooth crash. During the early phase, the Ar impurity profiles were hollow. A similar phenomenon was observed during laser ablation experiments in JET L-mode and H-mode ELM-free plasmas where SXR analysis indicated that sawtooth crashes facilitated impurity penetration into the plasma core [22, 23]. Later, sawtooth crashes correlated with flattened impurity density profile (1-3 sec in fig 5, also in fig.6). Impurity flattening after a sawtooth crash has been observed in several machines and with a large variety of impurities [24-28]. It was seen previously at JET, in

laser ablation experiments in ohmically heated plasmas where the confinement time of the impurity ions was several times longer than the sawtooth period [29]. Continuous core MHD modes (seen in fig.6, in between sawtooth crashes) also correlated with reduced core impurity density. The beneficial effect of continuous (m=1, n=1) MHD modes in removing impurities from the plasma core was also reported from ASDEX-Upgrade [18].

The effect of sawteeth and other MHD instabilities upon the impurity density profiles was studied primarily at low to moderated impurity injection rates, where the impurity radiation did not saturate the SXR signal. Radiation fluxes from two SXR cameras were analyzed to deduce the Ar density. The SXR emissivity was assumed to be constant on flux surfaces. The local emissivity ε_{SXR} can be written as a function of impurity density n_I and the electron density n_e as:

$$\varepsilon_{sxr} = \frac{n_e^2}{Z_D} L_D^{sxr} + n_e \sum_I n_I (L_I^{sxr} - \frac{Z_I}{Z_D} L_D^{sxr}) \; .$$

The first term describes the Bremsstralung radiation (for zero dilution), while the second term describes the radiation caused by each impurity, I, including the dilution of the main ion D. For the plasma core, the mean charge Z and the total SXR power coefficients L^{sxr} of each element mainly depend upon the electron temperature, T_e, where deviations from corona ionization equilibrium were determined by the impurity transport code STRAHL [19, 30]. The relevant atomic data were taken from the ADAS database [31] and the detection efficiency was calculated from the tabulated coefficients [32]. The SXR emission increased at the Ar puff (upper SXR trace in fig.5) indicating that Ar radiation dominated the SXR signal. The Ar densities were calculated by subtraction of an offset radiation from a fixed carbon concentration of 2%.

IV. IMPURITY PEAKING AND ELM OBSERVATIONS

In the fuelling phase the combination of Ar plus the strong Deuterium fuelling, a low pedestal pressure was established with a transition from type I to type III ELMs [11]. In the after-puff phase, as the edge cooling was reduced a transition back into type I ELMs occurred. The type I ELM-frequency decreased as the radiation rate increased [33]. In discharges with high Ar injection (as in fig.1), ELM-free periods (up to 0.5 s) were observed. Core impurity accumulation following type I ELMs was evaluated as a contributor to the confinement degradation from bolometry and from SXR data analysis. No correlation between central Ar accumulation and ELM activity was found.

SXR emission in the after-puff phase indicated that core impurity accumulation occurred independent of changes in the accumulation in the outer region (fig. 7). The central Ar density, $n_{AR}(0)$ in the after-puff phase increased by 30% in the discharge with ICRH (shown in fig. 5 and 6), whilst in a similar discharge without added ICRH, $n_{AR}(0)$ increased by 120% (fig. 7). Nevertheless, at a normalized radius of 0.7, the Ar density was the same in both discharges (fig. 7).

The SXR emissivity profiles indicated that the impurity density increased following type I ELMs. The increase occurred mostly in the outer region, within 20-30 cm from the edge (fig. 8). In the discharge with combined heating, the ELM frequency was 30% higher (fig. 7), however the region where the SXR increased was similar (fig.8).

Bolometer data analysis indicated that central impurity accumulation occurred in a variety of ELM regimes, including Type III ELMs (figure 9). In order to take into account the difference in ELM frequencies and amplitudes, we plotted in figure 10 the change in impurity concentration versus the integrated ELM amplitude observed in the after-puff phase. No correlation was found.

V. EXPERIMENTS TO CONTROL Q(0) AND MAINTAIN SAWTEETH

To keep q(0) below unity and maintain sawteeth, a small amount of ICRF power (1-3MW) was added to the main NBI heating. The RF heating resonance layer was located on axis to increase the central electron temperature. Low ICRF power was used in order not to create a significant population of ICRF accelerated ions, thus avoiding sawtooth stabilization by fast particles [34]. Hydrogen was used as the minority species, with the antennas operated either in dipole, or with –p/2 phasing. In both configurations the central T_e was increased ($DT_e(0) \sim 0.5$ kEV), preventing q(0) increasing as fast as in the reference discharges. In these experiments, sawteeth were maintained and the impurity profile didn't become as peaked as in discharges without added ICRH (figures 7 and 11).

Experiments with ICRH were performed at different Ar injection rates. At moderate injection rates ($\phi_{AR}=2x10^{21}$el/s in fig.7), although $n_{AR}(0)$ increased over 100% during the after-puff phase, the actual central Ar concentration was negligible ($C_{Ar}(0)\sim0.1\%$ for the discharges in fig. 7). The benefits of adding ICRH heating were observed at higher injection rates ($\phi_{AR}=4x10^{21}$el/s in fig. 11 and 12). With ICRH, the central Ar concentration was decreased and maintained at 1%, instead of 2% without ICRH. Loss of confinement and density were not observed (fig. 12). Thus in the discharge with added ICRH the high performance phase was extended and lasted in a quasi-steady state until the heating was turned off. In addition, there is no loss of confinement when compared to a non-seeded discharge.

VI. DISCUSSION

Experimental results indicated that sawteeth contributed to impurity control. SXR data analysis showed that central MHD instabilities, sawtooth crashes and, to a lesser extent continuous n=1 modes, prevented impurity peaking. However, other mechanisms affecting impurity transport may also have contributed to impurity control. Increasing power in the plasma core may prevent impurity accumulation in several ways. It maintains the central MHD instabilities and their beneficial effect in re-distributing impurities. In addition, a higher temperature would increase Ar ionization, leading to a decreased radiation from the central region. The improved power balance may avoid the impurity accumulative instability as suggested in [35].

Our main object in the experiments with ICRH was to keep the central q value below unity, maintaining the sawtooth instability. To achieve this, the ICRH was tuned, on one hand to increase the core current density, on the other hand to avoid creating the long sawtooth-free periods that are usually observed with ICRH [36]. In order to increase the central T_e the ICRH power was delivered on axis. However, large sawteeth can be created when ICRH heating is applied inside the q=1

region. Thus the ICRH power was deliberately kept low (2-3 MW). Adding ICRH has successfully prevented q(0) from rising above unity (figure 11). It has however not restored the peaked current density and the low q(0) values observed in the puffing phase.

Magnetic equilibrium calculations and MHD observations indicated that with ICRH, q(0)~1 (with q-profiles similar to those shown in figure 4, top). In addition to the sawtooth instability, a nearly continuous n=1 mode was observed. SXR data analysis indicated that both instabilities kept the impurity profile flat (fig. 6). The MHD stability including fast particle effects needs to be modeled and understood. Although a significant energetic ion component was not expected for densities so close to the density limit, the fast ion pressure inside the q=1 radius increased by 20-30%. Thus fast ion effects on the internal kink stability may be responsible for the increased sawtooth periods in the discharges with combined heating. [34]. (The power deposition of ICRH ions was studied using the analysis codes TRANSP [37, 38] and PION [39, 40].)

The impurity accumulation is often described by neo-classical theory [35]. Usually good agreement is found between the experimental derived transport coefficients and neo-classical theory, in periods between sawtooth crashes [18] and after sawtooth suppression [20]. The flux of the impurity ions can be described by diffusive and convective terms: $\Gamma_z = -D_z\, dn_z/dr + v_z\, n_z$.

In the presence of sawtooth relaxations the diffusive transport is thought to be increased due to profile flattening effects during the actual sawtooth crashes. Thus the sawtooth-period-time-averaged diffusion coefficient consists of neo-classical and sawtooth crash determined components, which contribute to $D_\perp$. On the other hand, if the convective transport is determined by neo-classical theory only, it is governed by the gradients of the ion density and ion temperature profiles [35].
In the JET experiments considered here, Argon was found to be in the Pfirsch-Schluter collisionality regime. It is shown in [35] that for neo-classical convection in the Pfirsch-Schluter regime, changes in the background ion density and temperature have opposite effects on the convection velocity. Impurity accumulation may be prevented by an increased grad (T_i), referred to as a "temperature screening". Impurity accumulation is governed by a competition between the stabilizing effect of impurity diffusion and heat conduction and the destabilizing effect of neo-classical convection and radiation. In the model described in [35], where strong coupling of Te and Ti and $D_\perp = 3n_i K_\perp$ is assumed, a critical density criterion for the development of impurity accumulation was given (equation 10 in [35]). This criterion was tested for pulse 46970, where impurity peaking occurred before the end of the puffing phase. The measured density was of the same order as the expected critical density. Increasing heating power in the plasma core would increase the central ion temperature. The temperature screening and the critical density for the accumulation instability would also increase.

In [35] a critical heating power density, Q_{crit}, is introduced, below which a development of the instability is expected: $Q_{heat} \le Q_{crit} = C\frac{D_{neo}}{D_\perp} Z_I Q_{rad}$. Q_{heat} and Q_{rad} are the central heating power and the central radiation power densities. C is a constant of order 1 that depends on profile effects, Z_I is the charge of the impurity, in our case of Argon not fully ionized: $Z_I \approx 16$ (for the Te observed in the

plasma core). (Note: There is a mistake in equation 11 of ref. [35], where Z_I is missing.).

In order to test this criterion, the power balance in the plasma core was studied (fig. 13), for the high Ar rate discharges compared in the previous section (figures 11 and 12). The heating power density was calculated using the analysis code TRANSP [37-38], while the radiative heating density was obtained from bolometry measurements. The critical power density Q_{crit} was estimated taking diffusion coefficients $\frac{D_{neo}}{D_{\perp}} \approx 0.2$ [41]. In the reference discharge (NBI only), Q_{rad} started to increase slowly at t~0.75 s. When the sawteeth disappeared, t>1.3 s, Q_{crit} exceeded Q_{heat}. Thus the sudden impurity accumulation that followed could be explained on the basis of the instability proposed in [35]. Also as proposed in [35], an increase of the heat power density would prevent impurity accumulation. When the heating power density was increased by ICRH, Q_{crit} was always below the actual heating power density Q_{heat} (fig. 13). However, more detailed analysis of the transport coefficients is required in particular in the ICRH discharges, where doubts remain if the convection velocity is purely neo-classical [40].

Experiments at TEXTOR [42] did show a similar beneficial effect of ICRH on the impurity accumulation behavior. At TEXTOR the transport of tungsten was investigated in neon RI-mode plasmas. Since Argon in JET plasmas was in the Pfirsch-Schlueter collisionality regime, the experiments with tungsten (always in Pfirsch-Schlueter regime in nowadays tokamaks) in TEXTOR RI-mode plasmas are a good comparison. It was found that ICRH leads to a broadening of electron density profiles and consequently to an outward directed neo-classical convective velocity, which suppresses accumulation effects. This is very similar to the convective velocity of argon in JET, which is also outward directed in discharges with ICRH [41].

One advantage of increased heating was to avoid radiative collapses that are sometimes observed. These limit the amount of Deuterium and Argon that can be used in the after-puff phase and may lead to disruptions. In fig. 13, the core radiation about equals the local heating power in the after-puff phase in the discharge with NBI heating. This local radiative collapse was not observed with added ICRH.

Power scans planned for future JET experiments will assess the advantages of increasing power with ICRH in comparison with increased NBI heating. A discharge with NBI power of 14 MW was produced for comparison with the combined heating discharge discussed above (figures 11-13). In this higher power, NBI only discharge, no impurity accumulation was observed, in spite of sawtooth suppression. However, the sawtooth was substituted by a continuous central n=1 mode that remained until the end of the heating phase. SXR analysis indicated that continuous central modes helped to prevent impurity accumulation. The effect of MHD modes on impurity transport coefficients needs to be better understood. In addition, this particular discharge had a central electron density 30% lower than in the discharges discussed above, making the impurity transport not comparable.

Larger ICRH powers, leading to Te(0)>5KeV, would imply a higher ionization degree for the impurities in the plasma core, with a large percentage of fully stripped Ar ions. In this situation the same Ar concentration would correspond to a decreased radiation from the centre (by a factor of

about 2 with Te(0)= 6KeV at the same electron density) [41]. Furthermore, at higher temperatures Argon is in the banana-plateau regime. In this case the proposed accumulation instability [35] cannot develop, since the balance between convective and diffusive transport contributions to the neo-classical transport will change. This is mainly due to the fact that D_{neo} decreases by going to higher temperatures and the temperature screening becomes less effective.

VII. CONCLUSIONS

Loss of confinement in discharges with high Ar injection rates was correlated with impurity accumulation in the plasma core. This was usually observed in the after-puff phase. Both edge and central MHD activity were assessed as contributors to performance degradation. No correlation was found between central impurity peaking and ELM activity. There was however a correlation between impurity density peaking and absence of sawteeth MHD activity. SXR data analysis indicated that the impurity density profile was flattened during sawteeth crashes. The impurity inflow into the central region was also reduced by continuous n=1 MHD modes observed when q(0)~1. Sawteeth were suppressed when q(0) rose above unity. After sawteeth suppression reversed shear q profiles were obtained.

Maintaining sawteeth by using ICRH resulted in quasi-steady state, high performance plasmas with high Ar densities. Values of $H_{97}*f_{GWD}$~0.8, previously only lasting less than 1 τ_E at high Ar injection rates, were now maintained for the duration of the heating phase ($\Delta t \sim 9\tau_E$). These experiments lead to the conclusion that the sawtooth MHD instability played an important role in preventing central impurity accumulation.

Future experiments and modeling should assess the role of increased central heating on impurity transport. In particular, it is necessary to find out how impurity transport coefficients are altered by sawtooth and other central MHD modes. Calculations of impurity diffusion coefficients, dealt with in a separate paper [41], concluded that ICRH leads to an outward directed neo-classical convective velocity.

REFERENCES

[1]. Weynants, R.R. et al., Nucl. Fus. 39 (1999) 1637

[2]. Vandenplas, P.E. et al, J. Plasma Physics 59 (1998) 587

[3]. G.H.Wolf et al., in Fusion Energy 1996 (Proc. 16th Int. Conf., Montreal, 1996), Vol. 1, IAEA, Vienna (1997) 177

[4]. Jackson, G.L et al., J. Nucl. Mater 266 – 269 (1999) 380

[5]. Ongena, J. et al, Plasma Phys. and Contr. Fus. 43 (2001) 12A

[6]. Dumortier, P. et al., submitted to PPCF (2002)

[7]. Maddison, J. et al., submitted to N.F. (2002)

[8]. Kubo et al. IAEA Conference in Sorrento, Italy (2000)

[9]. ITER Physics Basis Nucl. Fusion 39 (1999) 2175

[10]. Jackson, G.L et al., EPS Conference, Madeira, Portugal, 2001

[11]. Strachan, J. et al., Plasma Physics and Control Fus. 42, A81 (2000)
[12]. Keilhacker, M. and the JET Team, Nucl. Fusion 39 (1999) 209
[13]. Koslowski, R. et al, Plasma Phys. Control Fus. 39 (1997) B325
[14]. Koslowski, H.R. et al., EPS Conference, Madeira, Portugal, 2001
[15]. Post et al., At. Data Nucl. Data Tables 20, 397 (1977)
[16]. de Vries, P. et al., EPS Conference, Madeira, Portugal, 2001
[17]. Gehre, O. et al., Proc 14th European Conf. On Controlled Fusion and Plasma Physics, Madrid, part I, p. 156 (1987)
[18]. Dux, R. et al., Nucl Fus. 39 (1999) 1509
[19]. Guenter, S. et al., Nucl .Fus. 39 (1999) 1535
[20]. Rapp, J. et al., Plasma Phys. Contr. Fus. 39 (1997) 1615
[21]. Lao, L.L. et al., Nucl. Fusion 30 (1990) 1035.
[22]. Gianella, R. et al., Nucl. Fus. 34 (1994) 1185
[23]. Pasini, D. et al., Nucl. Fus. 30 (1990) 2049
[24]. Seguin, F., Petrasso, R. and Marmar, E.S, Phys. Rev. Lett. 51 (1983) 455
[25]. Petrasso, R. et al., Phys. Rev. Lett. 49 (1982) 1826
[26]. Hinnov, E. et al. Bull. Am. Phys. Soc. 25 (1980) 902
[27]. Ida, K. et al., Phys. Rev. Lett. 58 (1987) 116
[28]. Ida, K. et al., Plasma Phys. and Contr. Fus. 28 (1986) 879
[29]. Pasini, D. et al., Plasma Phys. and Contr. Fus. 34 (1992) 677
[30]. R. Dux, A. G. Peeters, Nuclear Fusion, Vol.40(10), 1721-1729 (2000)
[31]. B. L. Henke, E. M. Gullikson, and J. C. Davis, in Atomic Data and Nuclear Data Tables, Vol. 54, No. 2 (1993)
[32]. http://xray.uu.se/hypertext/henke.html
[33]. Jachmich, S. et al., EPS Conference, Madeira, Portugal, 2001
[34]. Porcelli, F., Boucher, D., Rosenbluth, M.N., Plasma Phys. Control. Fusion 38 (1996) 2163.
[35]. Tokar, M.Z. et al. Nucl. Fusion 37 (1997) 1691
[36]. Campbell, D.J., et al., Phys. Rev. Lett. 60 (1988) 2148.
[37]. Goldston, R.J. et al., J. Comput. Phys. 43 (1981) 61
[38]. Budny, R.V., Nucl. Fusion 34 (1994) 1247.
[39]. Erikson, L.-G., Hellsten, T. and Willen, U., Nucl. Fus. 33 (1993) 1037
[40]. L.-G. Erikson and T. Hellsten, Phys. Scripta 55 (1995) 70
[41]. Puiatti, M.E., et al., " Radiation pattern and impurity transport in Argon seeded ELMy H-mode discharges in JET", submitted to PPCF (2002)
[42]. J.Rapp et al., 2nd Europhysics Topical Conference on RF Heating and Current Drive of Fusion Devices (Brussels, Belgium, 20-23 January 1998) Europhysics Conference Abstracts 22A p89.

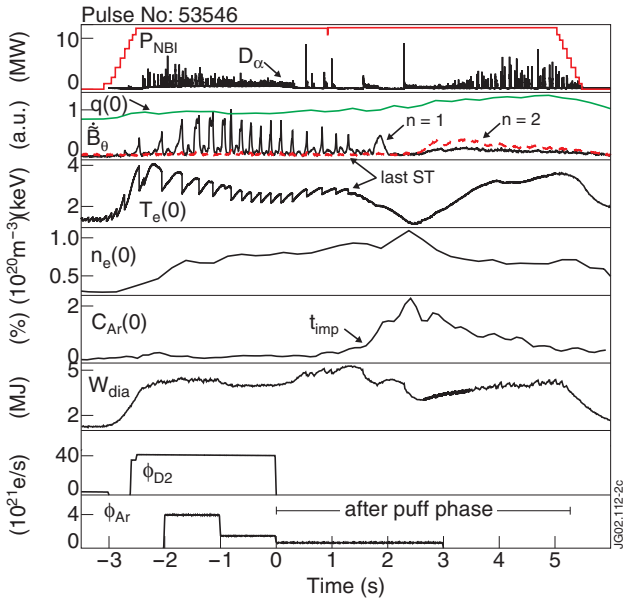

Figure1: Overview of a discharge with high Argon injection rate (P_{NBI} = 12 MW, I_p= 2.5 MA, B_T = 2.5 T). The boxes contain the following parameters plotted versus time, where t=0 sec is the start of the after-puff phase: a) Heating power and D_α emission showing the ELM behaviour. b) q on axis from EFIT, n=1 and n=2 magnetic perturbations. The spikes in the n=1 signal are sawtooth MHD precursors. c) Central electron temperature. d) Central electron density. e) Central Argon concentration from bolometry analysis. f) Plasma stored energy. g) Deuterium injection rate. h) Argon injection rate. In this discharge a low Ar rate is maintained in the after-puff phase.

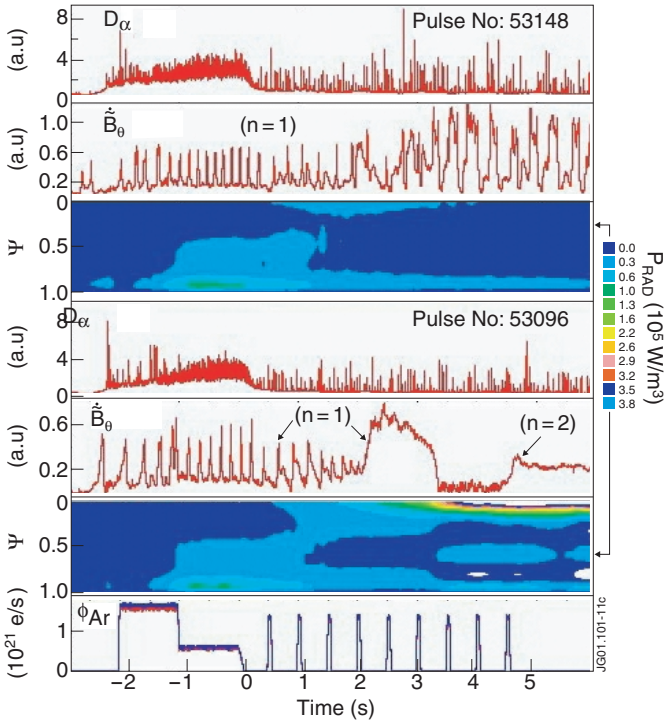

Figure 3: Comparison of discharges with low Ar injection rates showing different sawtooth observations in the after-puff phase. The boxes show the temporal evolution of D_α emission, magnetic pick-up coil signal, contour plot of the radiation power density (Abel inverted bolometer profiles) and Ar rate. Time = 0 sec is the start of the after-puff phase. In discharge 53148 with sawtooth crashes until the end of the heating phase, radiation peaking is not observed. In discharge 53096 with sawtooth suppression at t=2s, radiation peaking is observed. The peak value is outside the plotted scale.

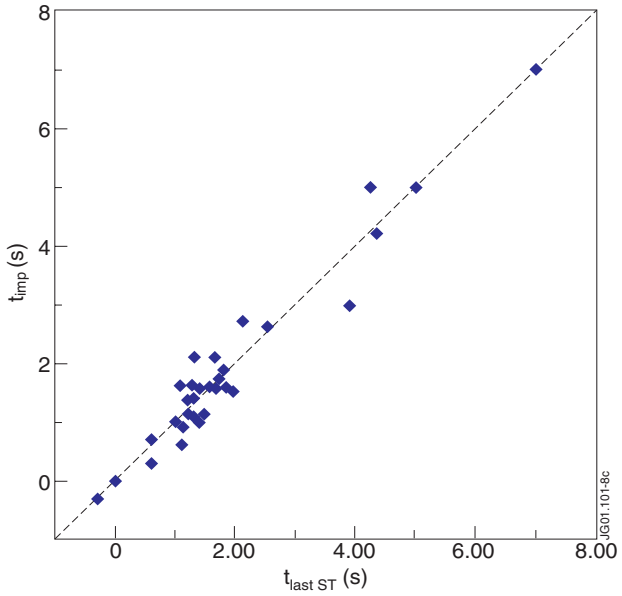

Figure 2: Time of sudden increase in central impurity concentration (t_{imp} in figure 1) versus time lastsawtooth crash is observed. For t ≥5s, sawteeth were maintained throughout the heating and no impurity peaking was observed, the time when the heating is off has been taken.

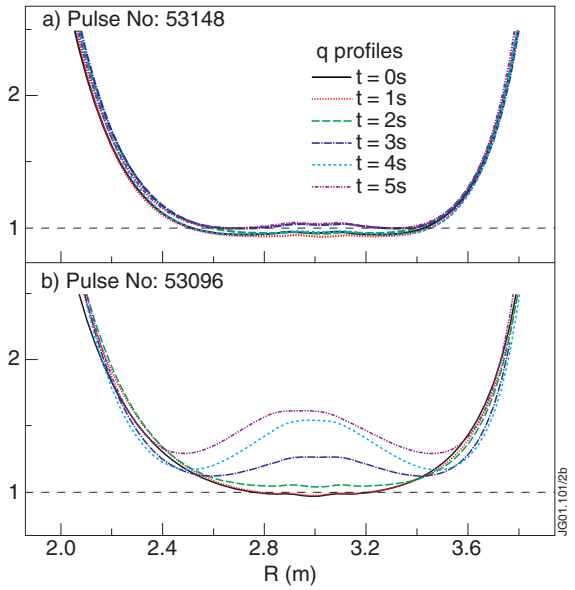

Figure 4: Magnetic equilibrium reconstruction including polarimetric measurements for the two discharges shown in figure 3. In the discharge with sawtooth present throughout the heating phase, the central q is nearly flat with q(0)~1. In the discharge with sawtooth suppression, reversed shear q-profiles are obtained after the sawtooth crashes stop (similar to observations in TEXTOR [12]).

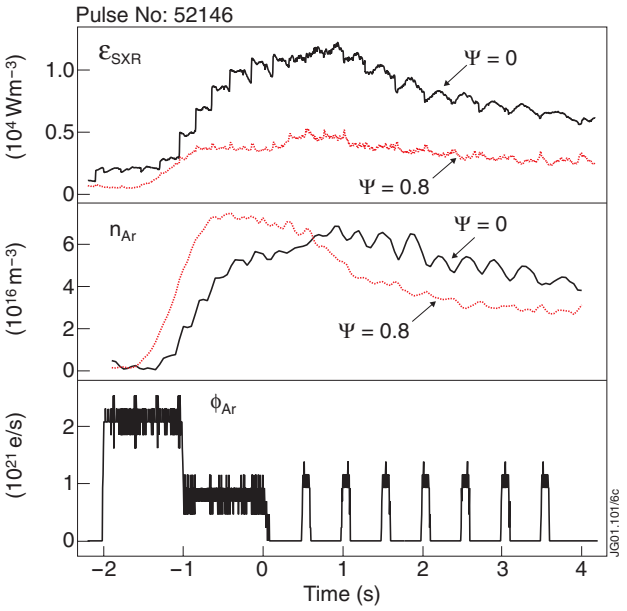

Figure 5:Central and edge SXR emissivity and corresponding impurity density deduced from SXR data plotted versus time, for a discharge with moderate Argon injection rate. In this discharge sawteeth were maintained by adding 3MW of ICRF heating to 12 MW NBI heating. In the puff phase the central SXR emissivity showed inverted sawteeth, indicating an increase in impurity level. In the after-puff phase, sawtooth crashes flattened the impurity density profile.

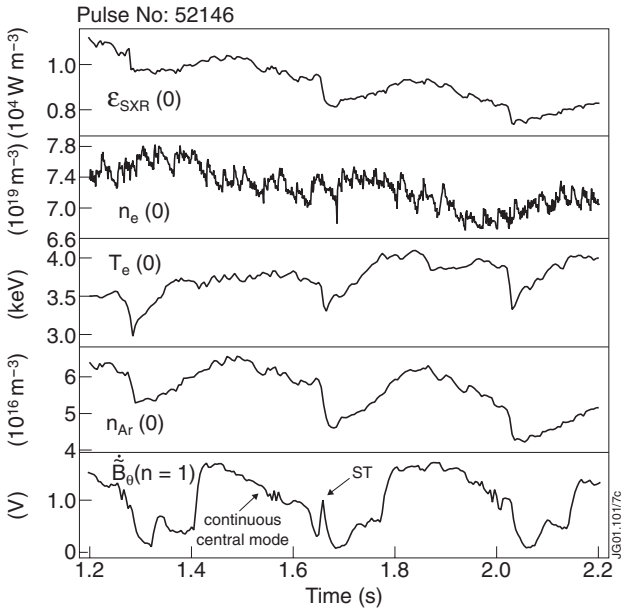

Figure 6: Same discharge as in figure 5. Central values of SXR emissivity, electron density and electron temperature and the derived Argon density plotted versus time during the after-puff phase. The bottom trace shows a magnetic pick-up signal. The central impurity density was reduced during continuous n=1 MHD modes and sawtooth crashes.

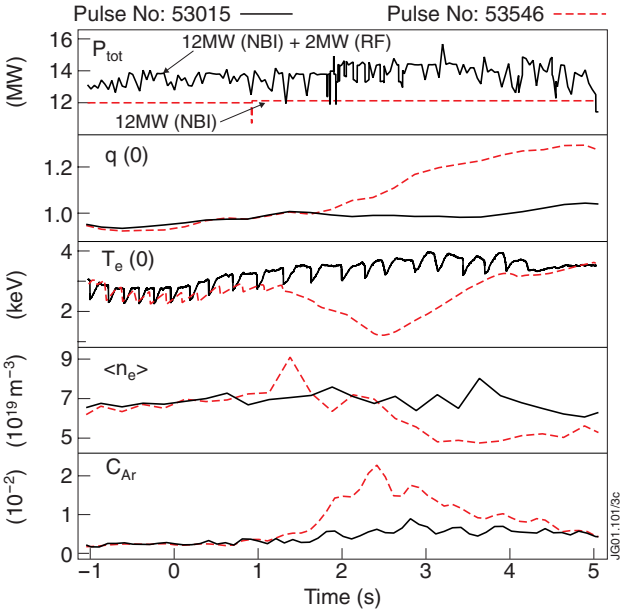

Figure 7: Argon density, D_α emission and electron temperature around the sawtooth inversion radii plotted versus time, for discharges 52144 (P_{NBI}=12 MW) & discharge 52146 (P_{NBI}=12MW+P_{ICRH}=3MW, see fig. 5 & 6). Time = 0 sec is the start of the after-puff phase. Sawteeth stop at t=1 s in the discharge with NBI only, while sawteeth are observed up to the end of the heating phase in the discharge with added ICRH. The ELM frequencies in the after-puff phase were f_{ELM}=30 Hz in the discharge with NBI only and f_{ELM}=45 Hz in the discharge with added ICRH.

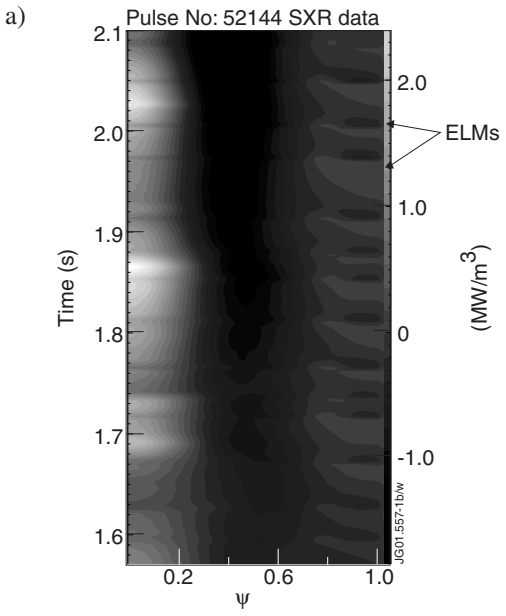

Figure 8a - Soft-X-ray emissivity profiles (with the average removed) for discharge 52144 (NBI only) after sawtooth suppression. Following type I ELMs the impurity density increases, however only in the outer region of the plasma (ψ>0.7).

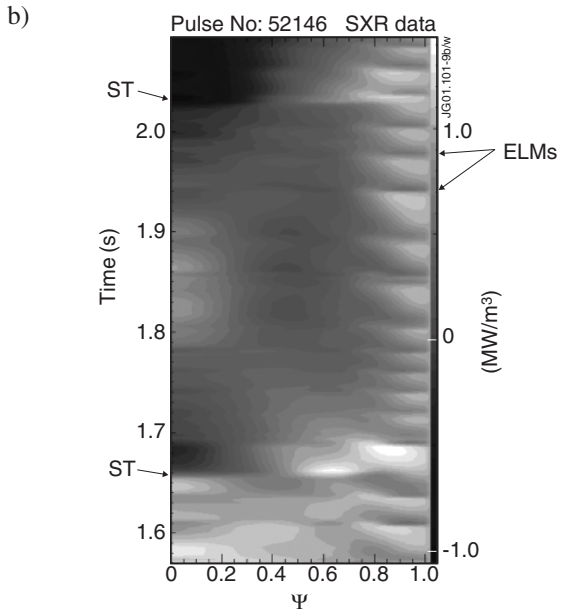

Figure 8b - Soft-X-ray emissivity profiles (with the average removed) for discharge 52146 (with combined heating). Following type I ELMs the impurity density increases, however only in the outer region of the plasma (ψ>0.7). The figure also illustrates the effect of sawteeth crashes on the central and outer SXR emissivity.

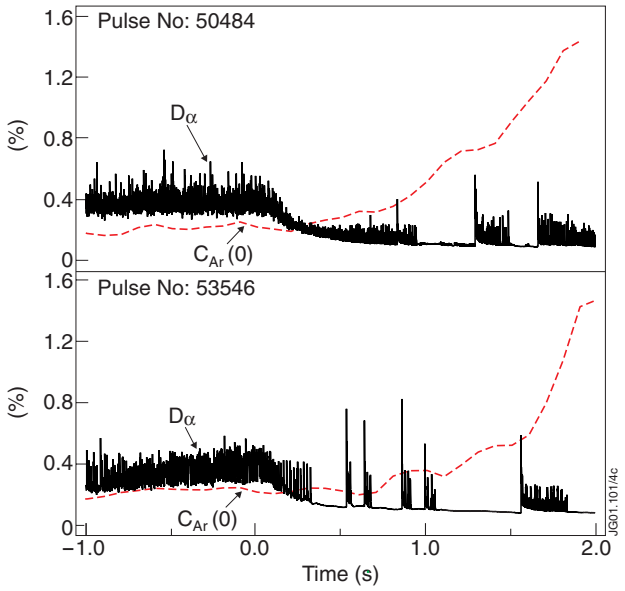

Figure 9 - Central impurity concentration (calculated from bolometer data analysis) and D_α signal versus time where t=0 s is the start of the after-puff phase for discharges with high Ar injection rates. In the first discharge the central Ar concentration starts to increase in the presence of type III ELMs. In the second discharge, central impurity accumulation starts following type I ELMs.

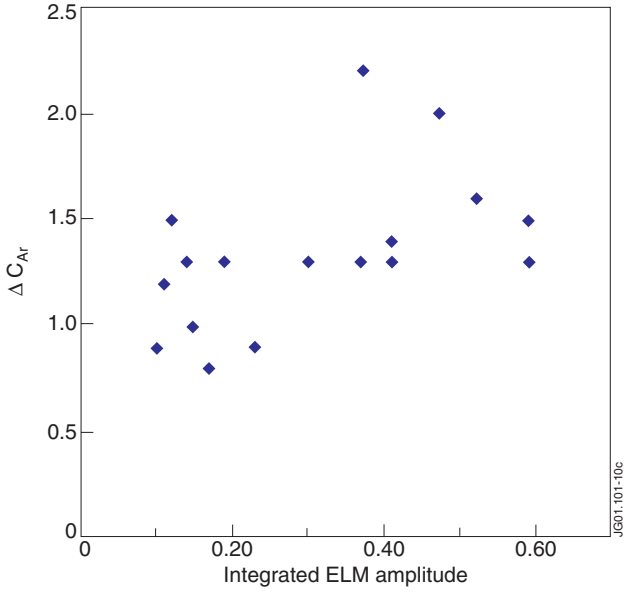

Figure 10 – Change in central impurity concentration observed in the after-puff phase plotted versus the integrated ELM amplitude. The integrated ELM amplitude is defined as the integrated D_α emission up to the time a sudden increase in central concentration is observed (t_{imp} in fig. 1).

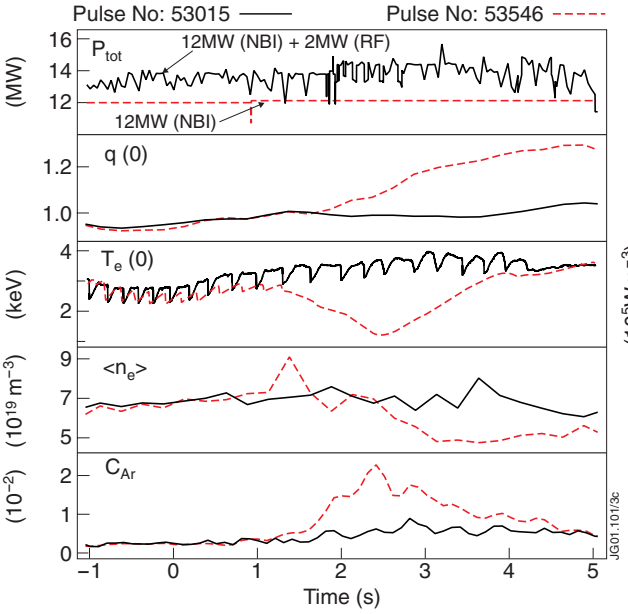

Figure 12: The product $H_{97}*f_{GWD}$ versus the number of energy confinement times, ntaue=time/τ_E, for the discharges shown in fig. 11. In the discharge with the sawteeth maintained, $H_{97}*f_{GWD}$ ~0.8 lasted for several confinement times.

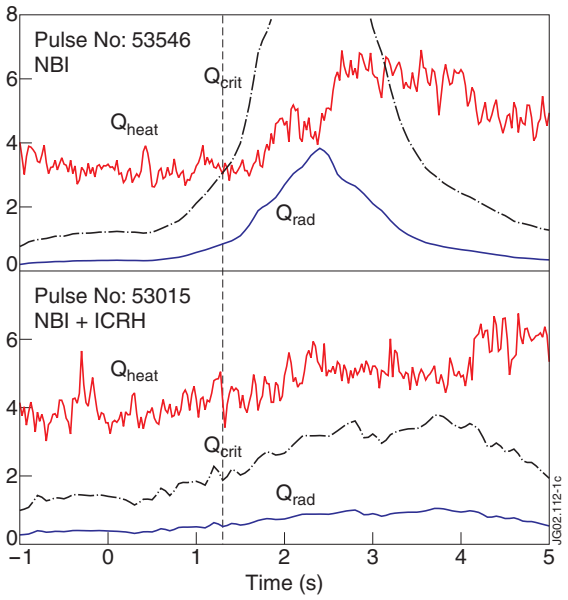

Figure 13: Volume averaged power densities at Ψ = 0.1 plotted against time, where t = 0 is the start of the after-puff phase. Q_{heat} is the heating power calculated by TRANSP, Q_{rad} is the radiated power measured by the bolometers. The critical power density, Q_{crit}, was estimated taking diffusion coefficients $\frac{D_{neo}}{D_{\perp}} \approx 0.2$. Sawteeeth in the discharge with NBI only (top) stopped at t=1.3s (indicated by dotted line, see also figures 1 and 12).